Int. J. Electrochem. Sci., 17 **(2022)** Article Number: 221028, doi: 10.20964/2022.10.45

International Journal of
ELECTROCHEMICAL
SCIENCE
www.electrochemsci.org

Preparation of N-doped Polypyrrole-derived Porous Carbon and Its Electrochemical Properties

Weibo Li[1], Shenglong Hu[1], Lili Wu[2], Xinguo Chen[2], and Heming Luo[2,]*

[1] Lanzhou Auxiliary Agent Plant Company Limited, Lanzhou New Area 730311, China.
[2] School of Petrochemical Technology, Lanzhou University of Technology, Lanzhou 730050, China.
[*]E-mail: luohm666@163.com

Received: 3 July 2022 / *Accepted:* 10 August 2022 / *Published:* 10 September 2022

Hyper-crosslinked polymers are inexpensive materials that have a high carbon content, making them ideal carbon precursor. In this study, hyper-crosslinked PPy was prepared by a solvothermal method. Using it as a precursor, N-doped porous carbon (PPyCN-800-B) was prepared by using urea, and the effects of the N doping ratio on the microstructure, components, and electrochemical properties of PPyCN-800-B were studied. The results demonstrated that PPyCN-800-1:4 was formed by the accumulation of non-hollow nanospheres of different diameters. The N content increased from 3.89% of PPyC-800 to 8.08%. When the current density was 1 A g^{-1}, the specific capacitance of PPyCN-800-1:4 increased from 109.1 F g^{-1} for PPyC-800 to 228.0 F g^{-1}, and the current density was increased from 1 A g^{-1} to 10 A g^{-1}, with a specific capacitance decay rate of 16.67% in 1 M H_2SO_4 electrolyte. After 5000 charging/discharging cycles, the capacitance retention was as high as 89.53%, showing the good cyclic stability and excellent electrochemical properties of PPyCN-800-B. N doping increased the number of porous carbon defects, produced more active sites with pseudocapacitance, and improved the material's wettability. This, in turn, facilitated the adsorption and desorption of electrolytic ions and significantly improved the electrochemical properties of porous carbon.

Keywords: hyper-crosslinked polymer; porous carbon; N doping; supercapacitor; specific capacitance

1. INTRODUCTION

Due to their good cyclic stability, excellent reversibility, and wide working temperature range, supercapacitors have attracted great attention in energy storage[1-3]. Porous carbon is inexpensive, has a wide source of precursors, controllable structure, and high electrical conductivity, and has potential application value in supercapacitors [4, 5]. Therefore, carbon materials research has recently sought resource-rich carbon precursors to develop new high-energy-storage carbon materials.

Porous polymers demonstrate the potential for good stability and synthetic diversification, but their poor electrical conductivity and low specific surface area limit their electrochemical applications

[6, 7]. Therefore, the development of energy-storage polymer derivatives has become a new research strategy. Polypyrrole α and β carbon atoms have similar binding energies, and they have a 3D morphology. Their structure displays obvious agglomeration and a low surface area, which is not conducive to its effective contact with an electrolyte, leading to the low electrochemical properties of polypyrroles [8]. Therefore, high-temperature carbonization of polypyrrole is typically performed to obtain a porous structure. N doping is also performed to increase active sites, induce redox reactions to obtain pseudocapacitance, improve the material's wettability, and increase the electrochemical properties of N-doped polypyrrole-derived porous carbon materials [9, 10].

Prakash *et al.* [11] prepared the porous carbon nanomaterial N-MCNR$_2$ by *in-situ* N doping, with a N content of 8.81%. It was used as an electrode material to prepare a supercapacitor in 1 M H_2SO_4 electrolyte. When the current density was 0.25 A g^{-1}, the specific capacitance reached 335 F g^{-1}, and the energy density reached 11.2 Wh kg^{-1}. After 50,000 cycles, the capacitance retention was 92.6%. Zhuo *et al.* [12] used aniline as the raw material to prepare a series of multi-level porous N-doped carbon nanotubes, which were used as a supercapacitor that showed excellent electrochemical properties. With 6 M KOH as the electrolyte, when the current density was 0.1 A g^{-1}, the capacitance reached 386.2 F g^{-1}. The above work has reference value for the preparation of heteroatom doped porous carbon materials and their energy storage research.

In this study, polypyrrole was taken as the carbon precursor and urea as the N source. Under an Ar atmosphere, direct carbonization was used to prepare N-doped polypyrrole-derived porous carbon, and the effects of carbonization temperature and N content on microstructure and electrochemical properties of the obtained porous carbon materials were investigated. This study provides experimental data for the study of N-doped polypyrrole-derived porous carbon materials and their applications in supercapacitors.

2. EXPERIMENTAL

2.1 Preparation of carbon precursor

First, 50 mmol of Pyrrole (Py), 100 mL of 1,2-dichloroethane (DCE), and 100 mmol of dimethoxymethane (FDA) were added into a 250 mL three-necked flask and stirred for 10 min. $FeCl_3$ (100 mmol) was added, condensed, and heated under reflux at 70 ℃ for 12 h. Then, the mixture was cooled, filtered, washed with methanol several times, and dried under vacuum at 70 ℃ for 24 h. The obtained solid was PPy (yield = 89.23%).

2.2 Preparation of N-doped porous carbon

The as-prepared carbon precursor PPy and urea were thoroughly ground in different mass ratios of 1: 3, 1: 4, and 1: 5. The mixtures were placed in a porcelain boat, placed in a high-temperature tube furnace, and heated to 800 ℃ under an Ar atmosphere at a rate of 5 ℃ min^{-1} and held at 800 ℃ for 2 h. Then, they were cooled to obtain a black solid product, which was washed with 1 M HCl several times and then washed with DI water until neutral. The black solid product was vacuumed at 70 ℃.

After drying for 12 h, N-doped porous carbon PPyCN-800-B was obtained. PPy is the carbon precursor, C is porous carbon, N is urea, 800 is the carbonization temperature, and B is the N doping ratio.

2.3 Characterization

The morphology and microstructure of the material were characterized by scanning electron microscopy (SEM, S-4800 LV) and transmission electron microscopy (TEM, Tecnai-G2). The pore structure of the material was characterized by a specific surface area analyzer (BET, Tristar II). According to the relative pressure (P/P_0) in the range of 0.06–0.20, the specific surface area of the test material was measured, and the pore size and pore volume were analyzed under a nitrogen atmosphere at P/P_0 = 0.97. The chemical composition of the material surface was analyzed by X-ray photoelectron spectroscopy (XPS, ESCALAB 250Xi). The surface morphology and elemental composition of the materials were tested by low-vacuum EDS mapping (JSM-5600 LV). An X-ray diffractometer (XRD, D/Max-2400) was used to analyze the characteristic peaks of the material in the 2θ range of 0-90° to clarify its crystal structure.

2.4 Preparation of working electrode

About 4 mg of the porous carbon material was mixed it with acetylene black and PTFE according to the mass ratio of 8: 1.5: 0.5. An appropriate amount of anhydrous ethanol was added dropwise to make it into a viscous shape, which was smeared evenly on the 1 cm × 1 cm Ni foam, vacuum-dried at 80 ℃ for 24 h, cooled, and pressed at a pressure of 12 MPa for 1.5 min to obtain the desired working electrode.

2.5 Testing of electrochemical properties

In this experiment, a three-electrode CHI660D electrochemical workstation was used to test the electrochemical properties of samples. In 1 mol L^{-1} H_2SO_4 electrolyte, PPyCN-800-B was used as the working electrode, a calomel electrode was used as the reference electrode, a Pt electrode was used as the counter electrode, and the operating voltage was from -1.0 ~ 0 V. Cyclic voltammetry (CV), galvanostatic charge-discharge (GCD) tests, and electrochemical impedance spectroscopy (EIS) were performed. A symmetric supercapacitor was assembled with PPyCN-800-1:4 as the positive and negative electrodes, and its electrochemical properties were tested using a two-electrode system.

The specific capacitance C (F g^{-1}) was obtained based on a tri-electrode electrochemical properties test [13]:

$$C = \frac{I \cdot \Delta t}{m \cdot \Delta V}$$

where I is the current density (A cm^{-2}); ΔV is the test voltage interval (V); m is the mass of active material in the electrode material (g); Δt is the discharge time (s).

3. RESULTS AND DISCUSSION

3.1 Phase analysis

3.1.1 Characterization of PPyCN-800-B by XRD

Figure 1 shows the XRD pattern of PPyCN-800-B, there are two characteristic peaks at 2θ ≈ 24.1° and 42.8°, which correspond to graphite's (002) and (101) crystal faces [14, 15]. Compared with standard graphite (2θ≈26.6°), the (002) diffraction peak of PPyCN-800-B shifted to the left because the interlayer spacing of carbon materials increased after N atom doping, resulting in lattice distortion. The broad diffraction peak in the figure indicated that carbon materials had many pores [16], which indicated that porous carbon materials were amorphous carbons with a low degree of graphitization [17]. The weak (101) diffraction peak of PPyCN-800-B indicated that the carbon materials had a low crystallinity because N doping caused the N atom at the defect formed on the surface of the carbon materials PPyCN-800-1:4 to remove electrons from the carbon layer. This produced more defects in the material and reduced its crystallinity [18].

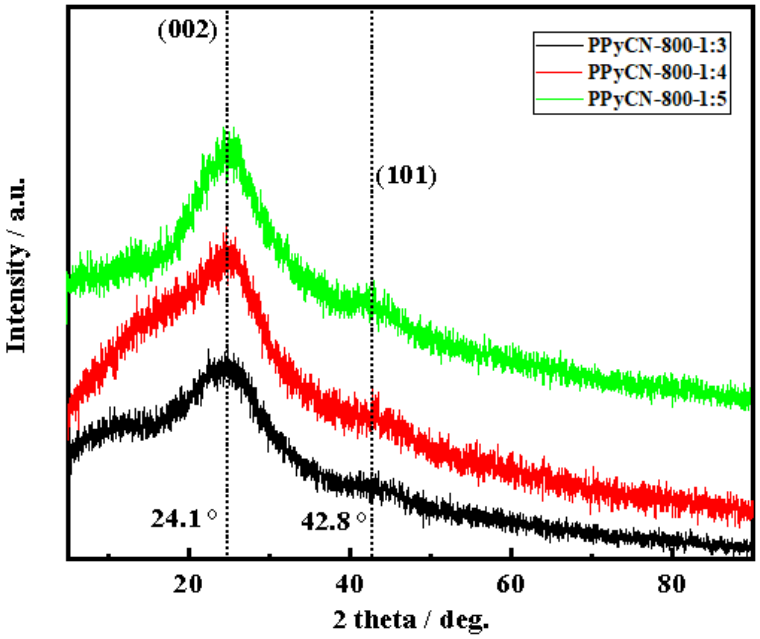

Figure 1. XRD of PPyCN-800-B

3.2 Microstructure

3.2.1 Morphology of PPy and PPyCN-800-1:4

Figure 2 (a, b) shows the SEM images of carbon precursor PPy formed by the accumulation of nanospheres with smooth and non-uniform surfaces. Figure 2 (c, d) shows the SEM images of the carbon materials PPyCN-800-1:4, which was formed by the stacking of nanospheres.

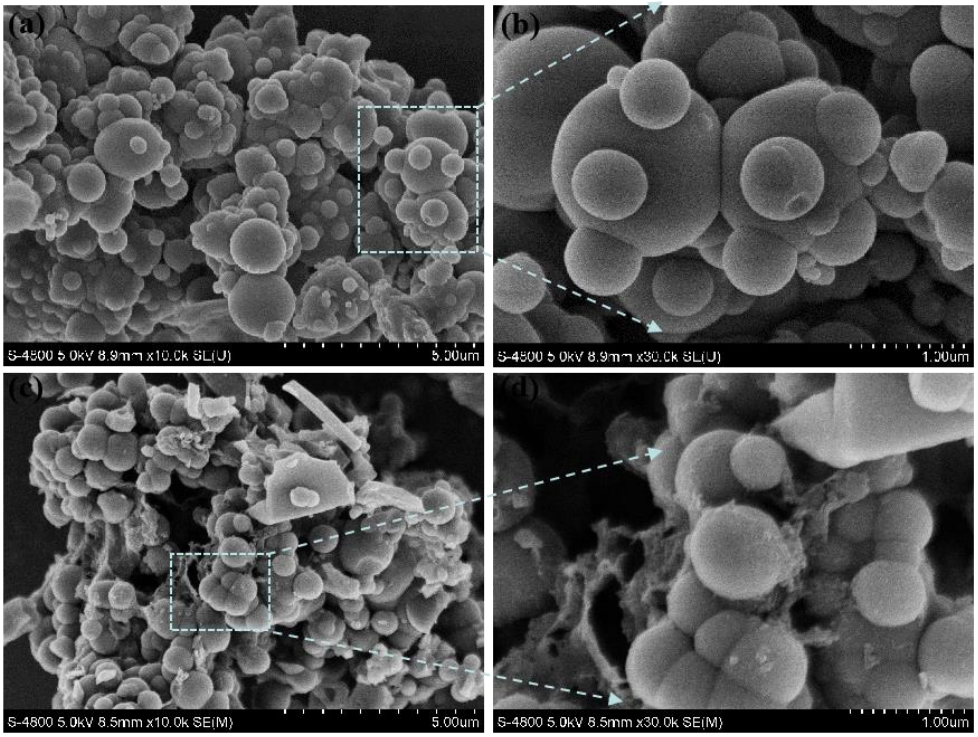

Figure 2. SEM images of porous carbon PPy (a, b) and PPyCN-800-1:4 (c, d)

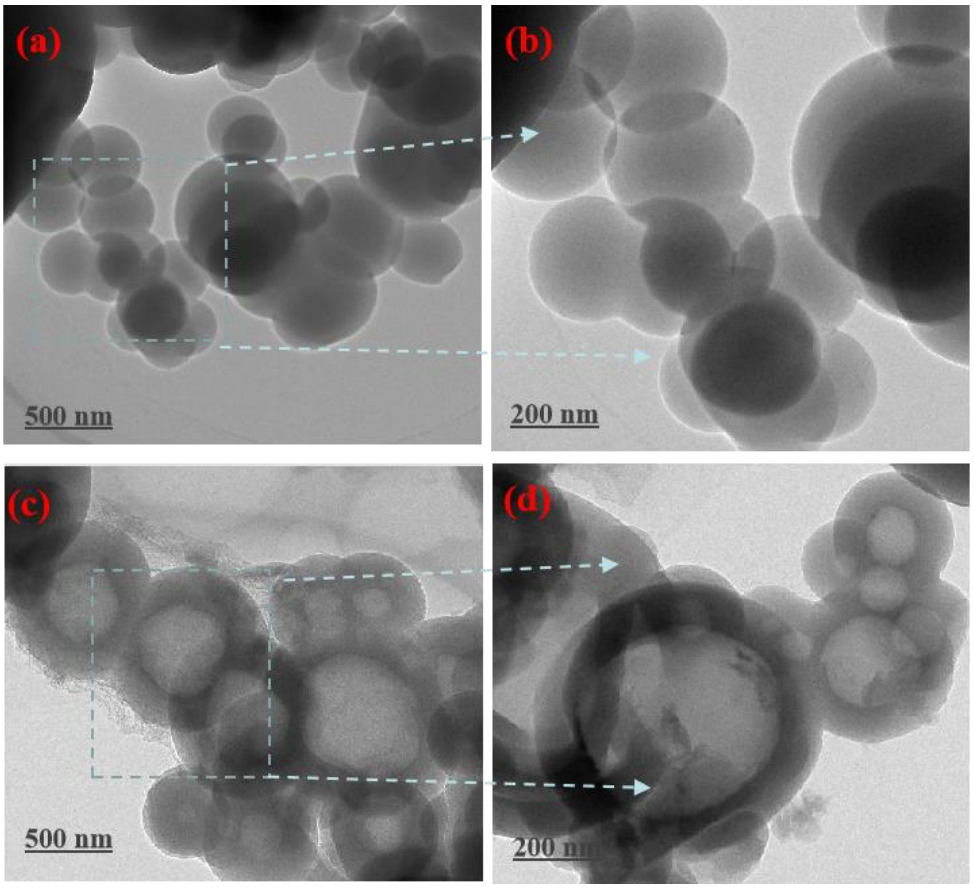

Figure 3. TEM images of porous carbon material PPy (a, b) and PPyCN-800-1:4 (c, d)

The surface of nanospheres was rough, and the surface contained a flocculent-like structure. The carbon precursor PPy was doped with urea so that the N atom was bonded to the surface of the PPyCN-800-1:4 nanospheres, and the N content increased. Figure 3 (a, b) shows TEM images of the carbon precursor PPy, which was composed of solid nanospheres with a smooth surface, which is consistent with the SEM images. Figure 3 (c, d) shows the TEM images of PPyCN-800-1:4, which is a hollow carbon material whose surface was wrinkled, flocculent, and rough, indicating that high-temperature carbonization hollowed out the PPyCN-800-1:4 spheres. N was successfully doped on the surface of PPyCN-800-1:4 nanospheres, which changed its structure.

3.2.2 BET analysis of PPyCN-800-B

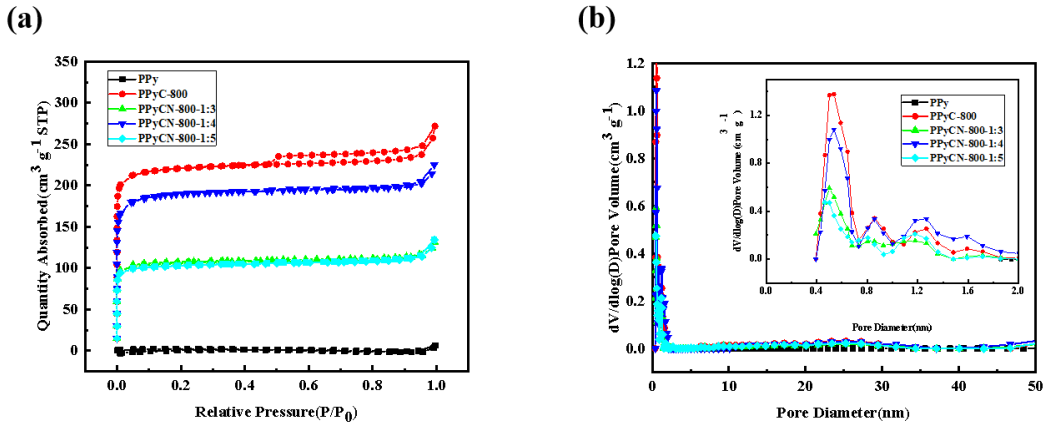

Figure 4. Nitrogen adsorption/desorption isotherms (a) and pore size distribution curves (b) of porous carbon PPyCN-800-1:4

Figure 4 shows the adsorption-desorption isotherms and pore size distribution curves of PPy, PPyC-800, and PPyCN-800-B under a nitrogen atmosphere. The carbon precursor PPy displayed a type II isothermal adsorption curve, and upon increasing the relative pressure, the adsorption curve became almost horizontal. This indicates that it had almost no pores, which is consistent with the conclusions drawn from the SEM and TEM images. PPyC-T displayed a type IV isothermal adsorption curve. When P/P_0<0.01, the gas adsorption increased rapidly, indicating that PPyC-T contained many microporous structures. When 0.01<P/P_0<0.95, the gas adsorption slowly increased, and an H_4-type hysteresis loop appeared. This was because the carbon precursor PPy underwent high-temperature carbonization, the carbon precursor PPy structure collapsed, and the carbon atoms rearranged to form mesopores, which increased the specific surface area of PPy-T. The adsorption-desorption curve of PPyCN-800-B was a type I isotherm. When P/P_0<0.01, the adsorption amount of N-doped porous carbon materials showed an upward trend due to the rapid filling of micropores by nitrogen, indicating that PPyCN-800-B had a microporous structure. When 0.01<P/P_0<0.8, a slight H_4-type hysteresis loop appeared in the adsorption isotherm, indicating that PPyCN-800-B contained some mesopores. When P/P_0 was close to 1.0, the adsorption capacity of PPyCN-800-B increased, indicating that the material

also had a macroporous structure. From the pore size distribution in Figure 4 (b), it can be seen that the pore size of PPyCN-800-B was mainly distributed around 1.7 nm, indicating that the pore structure was dominated by micropores, with a small number of mesopores. This is beneficial to the migration and transportation of ions in the electrolyte. Table 1 shows the specific surface area and pore parameters of PPyCN-800-B. As observed, upon increasing the urea doping ratio, the specific surface area and pore volume of porous carbon materials did not change significantly because the urea, under high-temperature conditions, decomposes into ammonia and CO_2. Compared with other literature, it was found that the specific surface area of PPy/N-PCM was much better than other PPy composites materials, for example: the specific surface area of CNW2-4 composite prepared by Wang et al. [19] was 580.2 m^2 g^{-1}. The N atom was partially bonded to the carbon atom, and CO_2 gas overflowed to achieve N doping.

Table 1. Specific surface area and pore parameters of PPyCN-800-B

Sample	S_{BET} (m^2 g^{-1})	S_{micro} (m^2 g^{-1})	S_{micro}/S_{BET} (%)	V_{total} (cm^3 g^{-1})	$D_{average}$ (nm)
PPy	6.01	4.46	74.21	0.001	0.98
PPyC-800	884.90	811.01	91.65	0.07	1.72
PPyCN-800-1:3	881.49	669.30	75.93	0.08	1.71
PPyCN-800-1:4	904.57	692.00	76.50	0.05	1.69
PPyCN-800-1:5	898.92	669.70	74.50	0.06	1.71

3.3 Surface composition and elemental analysis

Figure 5 shows the XPS spectra and elemental distributions of PPyC-800 and PPyCN-800-1:4. It can be seen from Figure 5 (a) and Figure 5 (i) that PPyC-800 and PPyCN-800-1:4 had characteristic peaks of C, N, and O elements, corresponding to C 1s binding energy peaks at 284.8 eV, an N 1s binding energy peak at 399.17 eV, and an O 1s binding energy peak at 532.25 eV, respectively. In PPyC-800 and PPyCN-800-1:4, the N and O element contents changed from 85.83% to 81.23%, 3.89% to 8.08%, and 10.28% to 10.69%, respectively. The carbon content of PPyCN-800-1:4 was slightly reduced after N doping, the N content significantly increased, and the oxygen content did not change significantly. Figure 5 (e-h) and (m-p) are C, N, and O element distribution maps of PPyC-800 and PPyCN-800-1:4. The porous carbon materials all contained a carbon backbone to which nitrogen and oxygen atoms were bonded. The surface elemental composition of porous carbon materials and construction type are key factors to the wettability of porous carbon materials. Nitrogen-containing and oxygen-containing functional groups induced a pseudocapacitance effect [20]. Figure 5 (b) is the C 1s spectrum of PPyC-800. The peaks at 284.7 eV, 285.4 eV, 287.7 eV, and 291.0 eV corresponded to C-C, C-N, C-O, and C=O groups, and their contents were 42.20%, 30.27%, 17.41%, and 10.12%, respectively. Figure 5 (j) is the C 1s spectra of PPyCN-800-1:4. The contents of C-C, C-N, C-O, and C=O groups were 38.78%, 33.49%, 18.12%, and 9.61%, respectively. As shown in Table 2, the C-N group content of PPyCN-800-1:4 increased by 3.22% compared with PPyC-800.

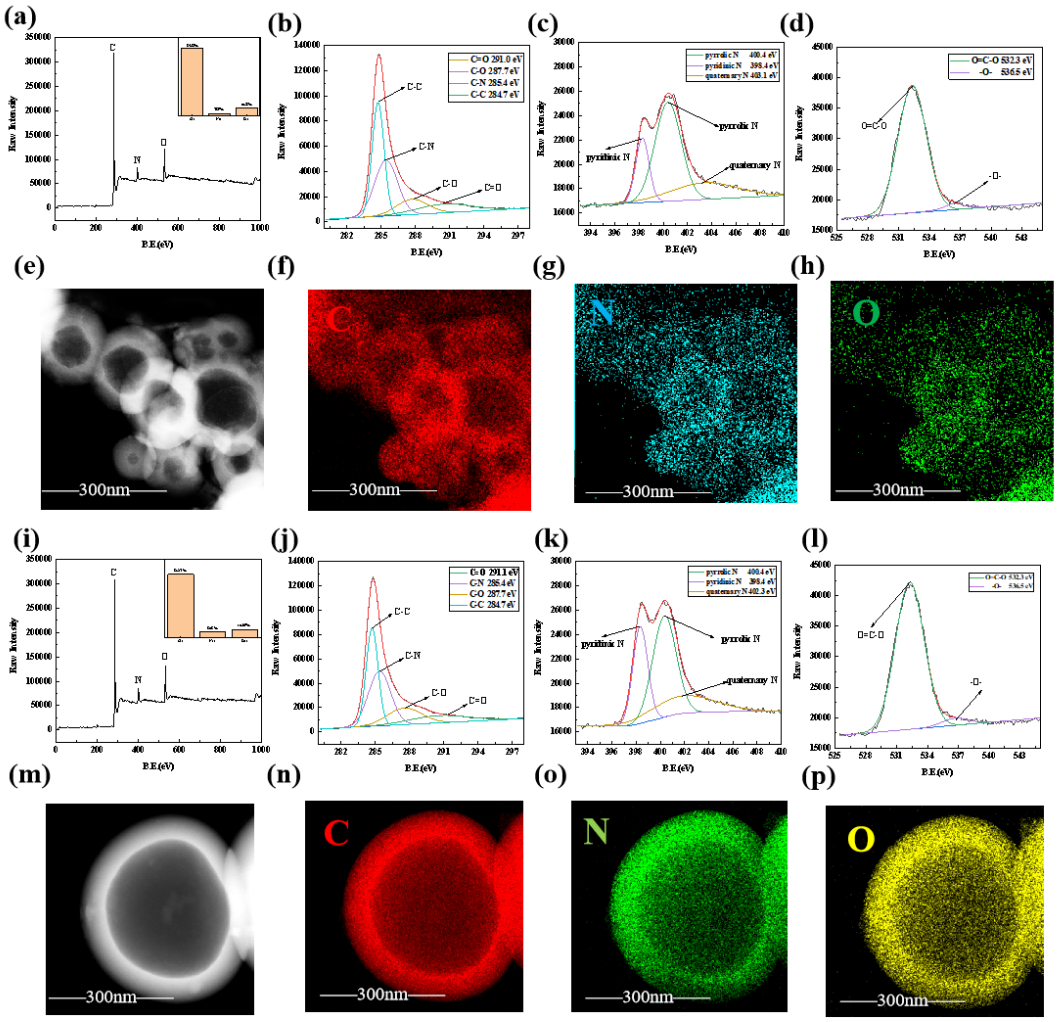

Figure 5. XPS spectra of PPyC-800 and PPyCN-800-1:4: full spectrum (a, i); C 1s (b, n); N 1s (c, k); O 1s (d, l); EDS element maps (e-h, m-p)

Figure 5 (c) shows the N 1s spectrum of PPyC-800. There were three distinct characteristic peaks with binding energies of 398.4 eV, 400.4 eV, and 403.1 eV, corresponding to pyridinic N, pyrrolic N, and quaternary N groups, respectively. The contents were 31.07%, 49.93% and 19.00%, respectively. Figure 5 (k) shows the N 1s spectrum of PPyCN-800-1:4, in which the contents of pyridinic N, pyrrolic N, and quaternary N were 40.13%, 46.56%, and 13.31%, respectively. It can be seen from Table 2 that the content of pyridinic N groups in PPyCN-800-1:4 was 9.06% higher compared with PPyC-800, and the pyrrolic N and quaternary N group contents were both reduced, indicating that the N atom in polypyrrole was converted into pyridinic N [20]. For PPyCN-800-1:4 surface defects, pyridinic N took some electrons from the carbon layer [21], thereby improving the wettability and electrochemical properties of the porous carbon materials. Figure 5 (d) is the O 1s spectrum of PPyC-800. There are two characteristic peaks with binding energies of 532.3 and 536.9 eV, respectively. The two peaks corresponded to O=C-O (83.19%) and -O- (16.81%) groups. Figure 5 (l) shows the O 1s spectrum of PPyCN-800-1:4. The contents of O=C-O and -O- were 84.13% and 15.87%, respectively. The oxygen content did not change significantly.

Table 2. XPS data of PPyCN-800-1:4

Element	Element classification	PPyC-800	PPyCN-800-1:4
C 1s	C-C	42.20	38.78
	C-N	30.27	33.49
	C-O	17.41	18.12
	C=O	10.12	9.61
N 1s	pyridinic N	31.07	40.13
	pyrrolic N	49.93	46.56
	quaternary N	19.00	13.31
O 1s	O=C-O	83.19	84.13
	-O-	16.81	15.87

By doping PPyCN-800-1:4 with N, the N content increased, in which pyridinic N dominated, which could induce a partial positive charge on the adjacent carbon. This changed the chemical properties of N-doped porous carbon materials and increased their electronic density of states, electrical conductivity, and electrochemical activity, thereby improving the energy storage performance of N-doped porous carbon materials [22].

3.4 Electrochemical properties

3.4.1 Electrochemical properties of PPyCN-800-B

Figure 6 shows the electrochemical properties of PPyCN-800-B. Figure 6 (a) shows GCD curves of PPyCN-800-B in 1 M H_2SO_4 at a current density of 1 A g^{-1}. As observed, the GCD curves exhibited an isosceles triangle-like shape, indicating the good charging/discharging performance of this porous carbon material. At a current density of 1 A g^{-1}, the specific capacitance of PPyCN-800-1:4 was 228.0 F g^{-1}, which was higher than that of PPyC-800 (109.1 F g^{-1}). This suggests that N doping enhanced the specific capacitance of the porous carbon materials. Additionally, the specific capacitance of PPyCN-800-B first increased and then decreased because upon increasing the urea ratio, the N content of PPyCN-800-B increased, the content of C-N bonds increased, and the active sites on the surface of carbon increased. This re-distributed the charge density, which helped attract charged N^+ electrons from the anode and improve the ionic mobility, thereby enhancing the interactions between the electrolyte and electrode, and improving the specific capacitance [23, 24]. Figure 6 (b) shows the specific capacitance decay curves of PPyCN-800-B under different current densities. When the current density increased from 1 A g^{-1} to 10 A g^{-1}, the specific capacitance decay rate of PPyC-800 was 38.59%, and the specific capacitance decay rates of PPyCN-800-B were 13.27%, 16.67%, and 52.59%, indicating that N doping increased the decay rate of porous carbon materials. This may be due to the instability of the surface functional groups of N-doped porous carbon materials [25, 26] or because the migration and transport of electrolyte ions damaged the N-containing functional groups.

Figure 6 (c) shows CV curves of PPyCN-800-B under a scanning rate of 10 mV s^{-1}. The CV curve of PPyCN-800-B exhibit a rectangular shape, showing that the porous carbon material mainly exhibited electric double-layer capacitance. The introduced N reacted with free electrons in the electrolyte to generate redox peaks, which provided partial pseudocapacitance, resulting in a larger CV curve integral area of PPyCN-800-B than that of PPyC-800. The corresponding specific capacitance was higher, which was consistent with the conclusions drawn from the GCD curve.

Figure 6 (d) is the Nernst plot of PPyCN-800-B. In the high-frequency region, the intercept of the impedance curve and the abscissa represents the equivalent series resistance, which reflects the internal resistance of the electrochemical system. In the high-frequency region, the semicircle reflects the charge-transfer resistance at the interface between the electrolyte and electrode. As the charge-transfer resistance value decreases, the charge transfer rate increases at the interface as the diameter of the arc decreases. In the low-frequency region, all curves were vertical, and the vertical characteristics showed pure capacitive behavior, indicating that the electrolyte easily entered the pores of the electrode. As observed, the equivalent series resistances of PPyCN-800-B were 0.76, 0.69, and 0.83 Ω, respectively, which did not change significantly compared with the equivalent series resistance (0.79 Ω) of PPyC-800.

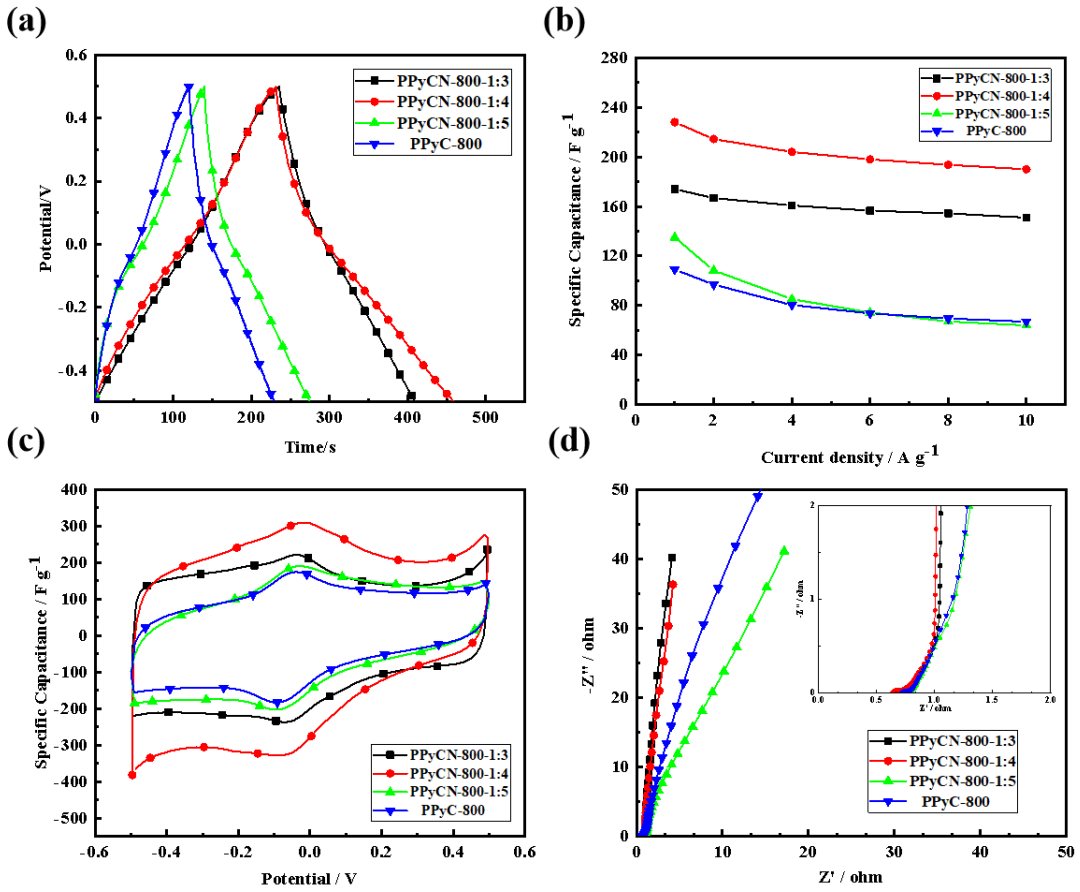

Figure 6. Electrochemical properties of PPyCN-800-B: GCD curve at a current density of 1 A g^{-1} (a); specific capacitance decay curve at different current densities (b); CV curve at a scanning rate of 10 mV s^{-1} (c); Nernst plot (d)

3.4.2 Electrochemical properties of PPyCN-800-1:4

Figure 7 shows the electrochemical curves of PPyCN-800-1:4. Figure 7 (a) shows GCD curves of PPyCN-800-1:4 in 1 M H_2SO_4 under different current densities. The GCD curves had a triangle-like shape, indicating the good charging/discharging performance of this porous carbon material.

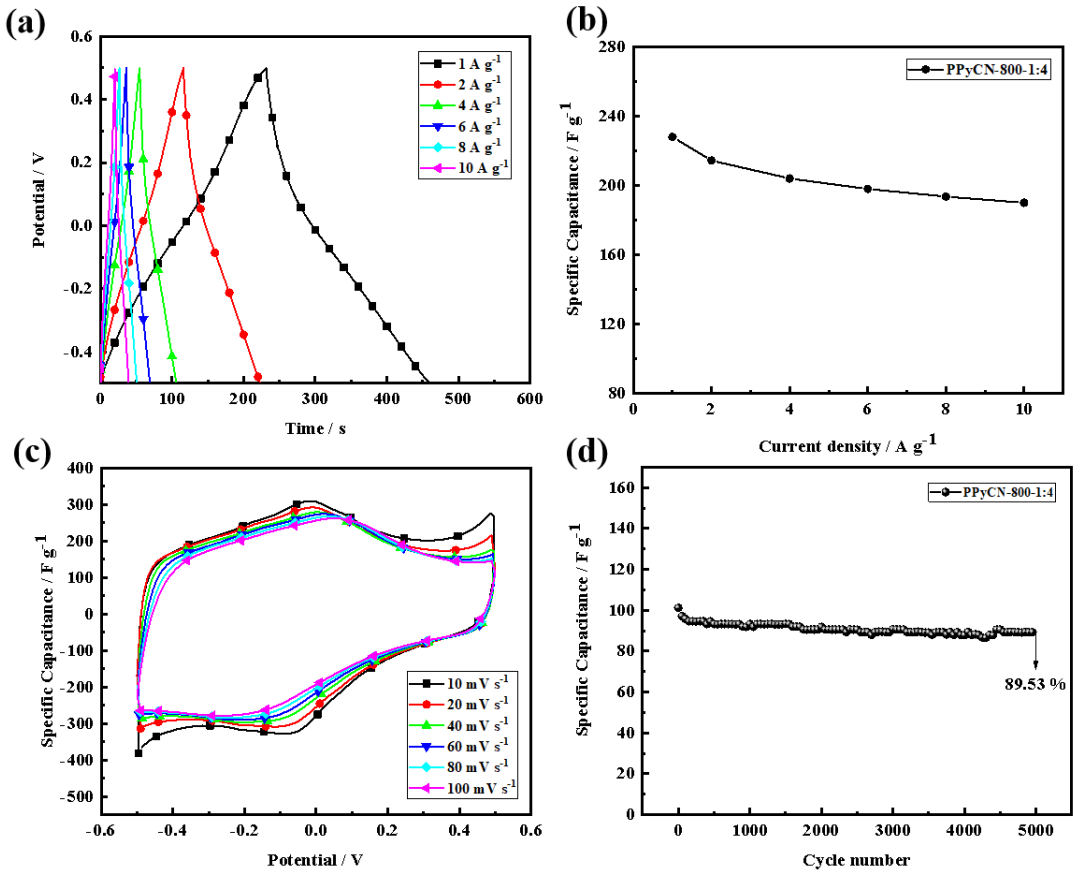

Figure 7. Electrochemical properties of PPyCN-800-1:4: GCD curves under different current densities (a); specific capacitance attenuation curve at different current densities (b); CV curves under different scanning rates (c); cyclic stability curve at a current density of 1.0 A g^{-1} (d)

At a current density of 1 A $g^{-1,}$ the specific capacitance of PPyCN-800-1:4 was 228.0 F g^{-1}, which was significantly higher than that of PPy (169.21 F g^{-1}) [27]. Comparison with other literature shows that the specific capacitance of PPyCN-800-1:4 doped with urea as the nitrogen source is better than that of other PPy composites. For example: Xu et al. [28] prepared PNCNT composites material with the specific capacitance of 174 F g^{-1}. The specific capacitance of the CNW2-2 composite prepared by Wang et al. [19] is 207 F g^{-1}. Figure 7 (b) shows specific capacitance decay curves of PPyCN-800-1:4 under different current densities. At a current density of 10 A g^{-1}, the specific capacitance decay rate of PPyCN-800-1:4 was 16.67%, demonstrating its good rate performance. Figure 7 (c) shows the CV curves of PPyCN-800-1:4 under different scanning rates, which showed a rectangular shape. A pair of redox peaks appeared due to the introduction of N, leading to redox

reactions. At a scanning rate of 100 mV s^{-1}, the N-doped porous carbon materials exhibited ideal capacitive behavior and efficient current responses. Figure 7 (d) shows the cyclic stability curves of PPyCN-800-1:4 at a current density of 2 A g^{-1}. After 5000 continuous current charging/discharging cycles, the capacitance retention was 89.53%. Superior to the capacitance retention of the ppy composite PPy/N-PCM made by Feng et al. [29]. The capacitance retention after 1000 charges and discharges was 88.53% of the initial capacitance value.

4. CONCLUSIONS

PPyCN-800-B was prepared by direct carbonization in Ar with PPy as the precursor and urea as the N source. The characterization results revealed that PPyCN-800-B was formed by the accumulation of hollow nanospheres with different diameters. The N contents of PPyCN-800-B and PPyC-800 were 8.08% and 3.89%, respectively. As the N content increased, the density of active sites on the surface carbon materials, as well as the ionic mobility, increased. Hence, the interactions between the electrolyte and electrode were enhanced, resulting in a higher specific capacitance. At a current density of 1.0 A g^{-1}, the specific capacitances of PPyCN-800-B and PPyC-800 were 228.0 and 109.1 F g^{-1}, respectively. At a current density of 10 A g^{-1}, the specific capacitance decay rate of PPyCN-800-B was 16.67%. After 5000 charging/discharging cycles, the capacitance retention of PPyCN-800-1:4 was 89.53%, demonstrating the excellent electrochemical properties of PPyCN-800-B.

ACKNOWLEDGEMENTS
This work was partially supported by funding from the National Nature Science Foundation of China (No. 22166023 and 21666018).

References

1. F. Béguin, V. Presser, A. Balducci and E. Frackowiak, *Advanced Mate rials*, 26 (2014) 2219-2251.
2. K. Fic, M. Meller and E. Frackowiak, *Electrochimica Acta*, 128 (2014) 210-217.
3. Y Tan, Y Liu, L Kong, L Kang and F Ran, *Journal of Power Sources*, 363 (2017) 1-8.
4. Z.S. Iro, *International Journal of Electrochemical Science*, 11 (2016) 10628-10643.
5. W. Raza, F. Ali, N. Raza, Y. Luo, K.H. Kim, J. Yang, S. Kumar, A. Mehmood and E. Kwon, *Nano Energy*, 52 (2018) 441-473.
6. J.M. Lee, M.E. Briggs, T. Hasell and A.I. Cooper, *Advanced Materials*, 28 (2016) 9804-9810.
7. A. Stein, Z. Wang and M.A. Fierke, *Advanced Materials*, 21 (2009) 265-293.
8. P.S. Sargin, L. Toppare and E. Yurtsever, *Polymer*, 37 (1996) 1151-1155.
9. C. Zhang, R. Kong and X. Wang, *Carbon*, 114 (2017) 608-618.
10. J. Han, G. Xu, H. Dou and D.R. MacFarlance, *Chemistry*, 21 (2015) 2310-2314.
11. P. Ramakrishnan and S. Shanmugam, *ACS Sustainable Chemistry & Engineering*, 4 (2016) 2439-2448.
12. T. Zhu, Z. Jin, Z. Li, S. Li, W. Si and S. Zhuo, *Journal of Materials Chemistry A*, 2 (2014) 12545-12551.

13. S. Zheng, J. Ma, Z.S. Wu, F. Zhou, Y. He, F. Kang, H. Cheng and X. Bao, *Energy & Environmental Science*, 11 (2018) 2001-2009.
14. X. Sheng, N. Daems, B. Geboes, M. Kurttepeli, S. Bals, T. Breugelmans, A. Hubin, I. Vankelecom and P. Pescarmona, *Applied Catalysis B: Environmental*, 176-177 (2015) 212-224.
15. Y. Cao, L. Xiao, M.L. Sushko, W. Wang, B. Schwenzer, J. Xiao, Z. Nie, L. Saraf, Z. Yang and J. Liu, *Nano Letters*, 12 (2012) 3783-3787.
16. Y.T. Pi, X.Y. Xing, L.M. Lu, Z.B. He and T.Z. Ren, *RSC Advances*, 6 (2016) 102422-102427.
17. X. Zhou, P. Wang, Y. Zhang, L. Wang, L. Zhang, Lan Zhang, L. Xu and L. Liu, *Journal of Materials Chemistry*, 5 (2017) 12958-12968.
18. F. Su, C.K. Poh, J.S. Chen, G. Xu, D. Wang, Q. Li, J. Lin and X.W. Lou, *Energy & Environmental Science*, 4 (2011) 717-724.
19. B. Wang, J. Qiu, H. Feng, S Eiichi and K. Takao, *Journal of Electroanalytical Chemistry*, 775 (2016) 219-227.
20. L. Qie, W.M. Chen and Z.H. Wang, *Advanced Materials*, 24 (2012) 2047-2050.
21. H. Yang, C. Zhang, Q. Meng, B. Cao and G. Tian, *Journal of Power Sources*, 431 (2019) 114-124.
22. Y. Zhao, J. Wan and H. Yao, *Nature Chemistry*, 10 (2018) 924-931.
23. M. Titash, K. Anil and K. Ramanan, *Chemistry of Materials*, 27 (2015) 716-725.
24. J. Zhang, J. Li, Z. Wang, X. Wang, W. Feng, W. Zheng, W. Cao and P.A. Hu, *Chemistry of Materials*, 26 (2014) 2460-2466.
25. Y. Xu, X. Qin, G. Zhang and Y. Zhang, *Fuel*, 253 (2019) 1317-1324.
26. H. Chen, J. Chen, D. Chen, H. Wei, P. Liu, W. Wei, H. Lin and S. Han, *Journal of Materials Science*, 54 (2018) 5625-5640.
27. Y. Chen, X. Zhang, C. Xu and H. Xu, *Electrochimica Acta*, 309 (2019) 424-431.
28. G. Xu, B. Ding, P. Nie, L. Shen, J. Wang and X. Zhang, *Chemistry*, 19 (2013) 12306-12312.
29. M. Feng, W. Lu, Y. Zhou, R. Zhen, H. He, Y. Wang and C. Li, *Sci Rep.*, 10 (2020) 15370.